Contact-based thymidylate transfer promotes collective tumor growth

Mohammad A. Siddiqui[1,5], Anne Mette A. Rømer[1,5], Luisa Pinna[1], Vignesh Ramesh[1], Sarah S. Møller[1], Paradesi N. Gollavilli[1], Adriana M. Turtos[1], Steffi Varghese[1], Lærke B. Guldborg[1], Nagendra P. Palani[2], Francesca Napoli[3], Marco Volante[3], Pawel Swietach[4] and Paolo Ceppi[1, 6,*]

[1]Department of Biochemistry and Molecular Biology, University of Southern Denmark; Odense, Denmark.

[2]Novo Nordisk Foundation Center for Basic Metabolic Research; University of Copenhagen, Denmark.

[3]Department of Oncology, San Luigi Hospital, University of Turin, Italy

[4]Department of Physiology, Anatomy & Genetics; University of Oxford, UK.

[5]These authors contributed equally

[6]Lead contact

*Correspondence. Email: pceppi@bmb.sdu.dk

Summary. Sustained cell proliferation is a fundamental hallmark of cancer, yet its mechanism remains elusive, particularly in context of intercellular cooperation and metabolite exchange. We uncover a mechanism of tumor growth via collective proliferation, where a syncytium of cells connected by gap junctions allows dTMP equilibration and dispenses ubiquitous activation of canonical dTMP biosynthesis and salvage driven by thymidylate synthase (TYMS) and thymidine kinase 1 (TK1) respectively. Collective proliferation is observed in vitro and in clinical samples, and it is validated in a genetic mouse model of lung cancer harboring dual *Tyms*/*Tk1* tumor-specific knockout, in which cells propel tumor progression despite lacking enzymatic dTMP synthesis, and the tumor growth is significantly mitigated by gap junction inhibition. These findings suggest that a programmed dTMP equilibration sustains collective tumor growth and revises the current dogma of a ubiquitous de novo activation. This mechanism could be exploited in cancer therapy.

Keyword. Collective cell proliferation, thymidylate, dTMP equilibration, pyrimidine metabolism, cancer

Introduction. Sustained cell proliferation, a key cancer hallmark, relies on a continuous supply of nucleotides either through multistep *de novo* biosynthesis or salvage of free nucleosides[1]. Consequently, oncogene-induced activation of nucleotide pathways is frequent in cancer[2,3] and is linked to cancer cell survival[4-7]. The current dogma of tumor growth emphasizes the universal activation of pyrimidine synthesis[8], thereby propagating an energy-exhaustive growth model.

Tumors are genetically heterogeneous entities[9] and the advent of high-end technologies have further resolved genetic and metabolic diversities at the single-cell level. Recent studies have shown that intercellular genetic heterogeneity caused by perturbation in the genes of fundamental metabolic pathways can be compensated by the equilibration of metabolites between electrically coupled cells forming a syncytium[10]. While xenobiotic perturbation of pyrimidine metabolism in cancer is a long-standing therapeutic strategy[11], genetic perturbations of pyrimidine genes observed in clinical samples[12,13] lack warranted attention. Therefore, we investigated proliferation dynamics using genetic perturbations of thymidylate synthase (*TYMS*, enzyme symbol TS) and thymidine kinase1 (*TK1*), which drive cell proliferation via the *de novo* synthesis and salvage of thymidylate (dTMP, thymidine monophosphate), the critical pyrimidine nucleotide involved in proliferation[8]. Our findings, along with *in vivo* modeling and clinical data, demonstrate the dispensability of intrinsically driven TS/TK1-dependent proliferation. Consequently, a new paradigm in tumor growth emerges that advances the current dogma and, therefore, has important therapeutic implications.

Intercellular dTMP transfer supports cancer cell proliferation. To establish a cell model devoid of *de novo* thymidylate synthesis, CRISPR/Cas9 was used to ablate *TYMS,* the gene coding the rate-limiting enzyme thymidylate synthase in cell lines (A549, Calu-1, and SK-MES-1) of non-small-cell lung carcinoma (NSCLC; **Fig S1A**). TS-KO reduced thymidylate levels, as quantified by mass-spectroscopy (**Fig S1B**). In line with the previous observation[14], TS-KO induced absolute growth arrest but was not lethal, and proliferated with supplementation of dTMP (thymidylate, deoxythymidine monophosphate, the product

of TS), but not by dUMP (deoxyuridine monophosphate, the substrate for TS) (**Fig S1C-E**). Furthermore, when testing different combinations of deoxyribonucleotides, only a combination containing dTTP (deoxythymidine triphosphate) promoted proliferation of TS-KO cells (**Fig S1F**). Morphologically, TS-KO cells were enlarged with senescence like features (**Fig S2A**), validated by high positivity for senescence markers, β-galactosidase (**Fig S2B**) and p21 (**Fig S2C**). Furthermore, knockdown of the salvage pathway gene TK1 minimally affected cell growth (**Fig S3A-C**), indicating that proliferation is primarily supported by TS-dependent *de novo* synthesis of dTMP. Thereby, TS-KO cells represent a growth-deficient cell model that is entirely dependent on exogenous dTMP for proliferation and was employed to investigate cellular dTMP perturbations.

Strikingly, proliferation in the TS-KO model was restored when cocultured with parental cells. This was demonstrated by knocking out *TYMS* in NSCLC cell lines that express nuclear H2B-GFP protein, followed by coculture with unlabeled parental cells and using real-time imaging (Incucyte S3) to exclusively monitor the proliferation of H2B-GFP TS-KO cells. In contrast to the TS-KO cells that failed to proliferate in the absence of exogenous dTMP, TS-KO cells proliferated in coculture with the parental cells (**Fig 1A, Fig. S4A**) and restored the normal morphology (**Fig 1B**). Since the quantification of the proliferative capacity of TS-KO cells was limited by the spatial constraint from proliferative parental cells, a long-term coculture was established and GFP expressing A549 TS-KO cells were flow sorted and counted after 10 passages in sub-confluent conditions. The sorted TS-KO cells failed to proliferate in absence of parental cells, proving the stable nature of dependency of KO cells on parental cells (**Fig 1C**).

Next, to determine whether deficiency of other nucleotides could be restored to regain proliferation, *RRM1* (to deplete all dNTPs) and *DTYMK* (to deplete pyrimidines) were knocked out in A549 cells (**Fig S5A**). The growth defect arising from nucleotide depletion was not restored in the coculture (**Fig S5B**), indicating the specificity of dTMP in collective proliferation. To further demonstrate that dTMP equilibration across the coculture causes the proliferation of TS-KO cells collectively with parental cells, parental dTMP donor A549 cells were cultured in L-Serine-3-^{13}C (Ser^{13C}) because serine's C-3 is transferred to dUMP to synthesize dTMP (**Fig S6A**). dTMP^{13C} enriched parental cells were then cocultured with puromycin-resistant TS-KO cells. Once the growth of TS-KO cells was restored, parental cells from the coculture were eliminated by puromycin treatment and dTMP^{13C} levels in

puromycin-resistant TS-KO cells from the coculture (**Fig 1D**) were quantified by mass spectrometry. Strikingly, dTMP levels were restored to levels measured in parental cells, along with dTDP and dTTP (thymidine diphosphate and triphosphate respectively, **Fig 1E**). Since neither serine supplementation nor puromycin-treated dead cells rescued TS-KO cell growth (**Fig S6B-C**), dTMP[13] detected in TS-KO must be acquired from the parental cells, indicating that equilibration of dTMP can rescue growth defect caused by perturbation of *de novo* dTMP synthesis to collectively support cell growth. However, to determine if this equilibration is also functional *in vivo*, TS-KO cells were subcutaneously injected with or without parental cells into the flanks NSG mice. TS-KO cells formed tumors even in the absence of parental cells (**Fig 1F**) indicating that collective proliferation is a fundamental mechanism and supported growth irrespective of lineages. Indeed, normal lung cells BEAS2B restored the growth of TS-KO cells *in vitro*, as well as Calu-1, a NSCLC cell line of different origin (**Fig 1G**).

The investigation was expanded to other non-epithelial cells previously associated with nucleoside secretion[15-17]. Of these, tissue-resident fibroblasts (**Fig S7A**), cancer-associated fibroblasts (CAFs, **Fig S7B**) and T lymphocyte cell line Jurkat cells (**Fig S7C**) failed to restore growth in TS-KO cells. However, among different the monocyte lineages tested (**Fig 1H**), THP-1 monocytes, M0 and M2 macrophages rescued the growth defect in TS-KO cells, whereas M1 macrophages did not (**Fig 1I**). Considering that protumor M2 macrophages support TS-KO cell growth and that cancer cells polarize macrophages to a M2-like phenotype (tumor-educated macrophages, TEMs) to secrete pyrimidines[18], we examined whether cancer cells can educate macrophages to support their growth. Therefore, A549 cell culture medium was administered to M0 macrophages to polarize them to TEMs. Conditioned medium was then collected from the TEMs and supplemented with fresh cell-culture medium for TS-KO cells (**Fig S7D**). While TEMs had a positive effect on TS-KO proliferation (like M2 macrophages), conditioned medium from the same TEMs did not facilitate TS-KO cell proliferation (**Fig S7E**). Despite nucleosides being secreted into the extracellular space and taken up by neighbor cells[18], our observations imply that dTMP sharing involves non-secretory routes. Accordingly, supplementing TS-KO cells with conditioned medium from parental cells was not sufficient to reestablish TS-KO cell proliferation (**Fig 1J**). Therefore, physical contact between TS-KO and dTMP donor cells is essential for TS-KO cell growth. To support this hypothesis, A549 cells were seeded on a

transwell-membrane that was impermeable to mammalian cells but allowed sharing of medium with KO cells. Unlike the stimulatory effect in contact-enabling coculture, the contactless setting in transwells failed to restore TS-KO cell growth (**Fig S7F**).

To summarize, senescent TS-KO establishing direct contact with viable surrounding cells (Fig S6C) to acquire dTMP and restore proliferation. These observations highlight the dispensability of *de novo* pyrimidine synthesis for growth. Importantly, we have identified a new collective model of proliferation that is relayed by equilibration of dTMP (produced by a subset of cells) through an interplay of cells of different lineages.

Collective Proliferation in patients with lung cancer. The concept of collective proliferation prompted a reconsideration of cancer cells scored null for TS in clinical samples[12,13] and explore their proliferative fates. Although dTMP is not reported in extracellular space, cells salvage thymidine and phosphorylate it to dTMP by TK1[19], which is further phosphorylated to dTTP to generate the dNTP pool required for DNA synthesis and proliferation (**Fig 2A**). Therefore, to restrict our analysis to cells devoid of any dTMP source, TS and TK1 expression were evaluated in single-cell RNA-seq data from patients with NSCLC[20].

Single cells of 40 NSCLC biopsies were pooled, clustered in different cell types and cancer cells were identified (**Fig S8A**). A significantly large number the cancer cells lacked expression of genes *TYMS* (expressing TS) and TK1 ($TYMS^{-}TK1^{-}$) in the cancer cluster (**Fig 2B**). In some patients $TYMS^{-}TK1^{-}$ cells contributed up to 80% of the total cancer cells (**Fig 2C**). Cancer cells were further classified based on the expression of the proliferation maker *MKI67*, and samples with more than 50 proliferative cells were analyzed. Remarkably, in some samples up to 50% $TYMS^{-}TK1^{-}$ cells were positive for *MKI67* (**Fig 2D**), highlighting their significant contribution to tumor growth. Furthermore, $TYMS^{-}TK^{-}$ cells frequently expressed other proliferative genes along with basic metabolic genes (**Fig S8B**), indicating the non-quiescent nature of these cells. When characterized further, the $TYMS^{-}TK1^{-}$ cells were differentially regulated compared to the cells expressing either *TYMS* or *TK1*, or both. As expected, the pyrimidine pathway was downregulated, and senescence signature was upregulated in $TYMS^{-}TK1^{-}$ cells. Also, the signatures for phenomena driving cancer pathology such as epithelial-mesenchymal transition[21,22] and inflammation[23,24] upregulated in $TYMS^{-}TK^{-}$cells (**Fig 2E**). *In vitro,* NSCLC cells with genetic

ablation of TS and TK1 (TS-TK1-KO), which underwent senescence like TS-KO cell, restored growth in the presence of parental cells (**Fig S9A-E**), indicating their dependency on dTMP donors for proliferation. Since collective proliferation is not mediated via passive diffusion of dTMP (Fig 1), a spatial NSCLC transcriptomic dataset was analyzed to evaluate interaction of *TYMS*$^-$*TK1*$^-$ cells with other populations. As would be expected for collective proliferation, *TYMS*$^-$*TK1*$^-$ cells (approximately 17% of the total cells) were found dispersed within other populations (**Fig 2F, Fig S10A**). A neighborhood analysis performed by calculating the proportion of different cell populations in successive radii (**Fig 2G**) revealed that *TYMS*$^-$*TK1*$^-$ were enriched in the vicinity of *TYMS*$^+$*TK1*$^+$ cells (**Fig 2H**). Meanwhile, these observations were not found in the *TYMS*$^-$*TK1*$^+$ and *TYMS*$^+$*TK1*$^-$ populations, but *TYMS*$^+$*TK1*$^+$ showed an opposite trend, i.e. exclude pairing with other *TYMS*$^+$*TK1*$^+$ cells (**Fig S10B**). Overall, these data support the notion that dTMP deficient cells can proliferate *in vivo* and contribute to tumor mass by obtaining dTMP from their surrounding cells.

dTMP exchange is mediated through gap junctions. Having established that physical contact between cells is necessary for collective proliferation, the next step was to investigate the molecular nature of this coupling. RNA sequencing showed that *GJA1* and *GJD3* were upregulated in growth-deficient and proliferative TS-KO cells, when compared to control cells (**Fig S11A**). *GJA1* and *GJD3* code for proteins Connexin43 (Cx43) and Connexin30.2 (Cx30.2), respectively. Cx43 and Cx30.2 can hexamerize to form gap junctions between cells, which generates a syncytium for intercellular metabolite exchange and may underpin the growth rescue effect[25,26]. Theorizing that TS-KO cells increased expression of gap junctions as supply lines for dTMP in coculture settings, the possibility that these cells are diffusively coupled was tested by fluorescence recovery after photobleaching (FRAP). Specifically, a monolayer of NSCLC cells was stained with calcein red-orange AM (size comparable to thymidylate), and a single cell randomly selected in a cluster was bleached within its limits. The post-bleaching recovery of fluorescence was recorded in the bleached cell. Results indicated strong recovery that was blocked in the presence of carbenoxolone (CBX), a pan-gap junction inhibitor, implicating gap junctions as pathways for diffusion (**Fig 3A, Fig S11B**). Further treatment of cocultures with CBX significantly reduced the growth of TS-KO cells at a concentration that has no detrimental

effect on the proliferation of the parental cells (**Fig 3B, Fig S11C-D**). In contrast, inhibition of nanotunnels (that form another mode of intercellular communication) by SMIFH2[27] did not reduce TS-KO cell growth in coculture (**Fig S11E-F**). CBX also inhibited the growth of spheroids composed of A549 TS-KO cells and parental cells, compared to the vehicle control (**Fig 3C, S11G**). Similarly, CBX treatment prevented THP-1 monocytes from restoring TS-KO cell growth (**Fig 3D**). Together, these data confirm gap junction-mediated cell coupling as the route for dTMP transfer.

Since RNAseq data identified *GJA1* and *GJD3* as the main candidates for forming connexins, their protein levels were quantified in KO cells. Expression of Cx43 (encoded by GJA1) was significantly increased in dTMP-deficient TS-KO and TS-TK1-KO cells, compared to the parental cells, as confirmed by Western blots (**Fig 3E**) and Cx43 immunofluorescence staining (**Fig 3F, Fig S12A**). Cx43 expression was also increased in proliferating KO cells (**Fig 3G**). Immunofluorescent staining of donor A549 cells from coculture with TS-KO showed that the parental cells also increased Cx43 expression (**Fig S12B**). Therefore, Cx43 was postulated to be the key connexin involved in dTMP equilibration; consequently, the absence of Cx43-mediated coupling was hypothesized to abolish the proliferation of TS-KO cells in coculture. Based on *GJA1* mRNA expression (**Fig S12C**), cells with undetectable levels of *GJA1* were identified for further studies. After confirming the lack of Cx43 expression by western blot (**Fig 3H)**, NCI-H1299 and NCI-H520 cells were cocultured with TS-KO cells. Whereas Calu-1, a Cx43-expressing line like A549, restored growth (**Fig 3I)**, Cx43-negative cells (NCI-H1299 and NCI-H520) failed. To further validate the role of GJA1, siRNA-mediated knockdown of GJA1 was introduced into TS-KO cells, as well as in A549 and Calu-1 cells that were used as dTMP donors. While GJA1 knockdown did not affect parental cell growth (**Fig S12D-E**), it significantly reduced the growth of TS-KO cocultured with A549 or Calu-1 cells (**Fig 3J**). This finding confirms GJA1 as the major channel of dTMP equilibration.

Gap junction-dependent *Tyms*$^{-}$*Tk1*$^{-}$ tumor growth *in vivo*. To test whether cells lacking *de novo* and salvage dTMP synthesis can form tumors *in vivo*, C57BL/6 ROSA-LSL-Cas9 mice[28] were delivered lung-tropic adeno-associated viruses (AAV) carrying gRNAs for humanized *Kras*^{G12D} mutation, *p53*, *Tyms*, and *Tk1* (*Kras*^{G12D}*p53*$^{-/-}$*Tyms*$^{-/-}$*Tk1*$^{-/-}$, KPTT; **Fig 4A, S13A**). Mice with *Kras*^{G12D}*p53*$^{-/-}$ (KP) derived tumors[29] were used as controls. Tumors

grew in the lungs of intubated KPTT mice (**Fig 4C**), and dTMP deprivation of a cell line derived from a KPTT tumor halted cell growth (**Fig 4D**) and displayed a senescent morphological phenotype associated with dTMP deprivation (**Fig 4E**). These findings indicate that *in vivo* cell growth depends on an extrinsic source of dTMP. Furthermore, dTMP-deprived cells formed tumors in the flanks of C57BL/6 mice, confirming their tumorigenicity despite the lack of intrinsic dTMP synthesis (**Fig 4F**).

Next, KPTT cells were cocultured with a syngeneic cell line Ladi 2.1 (derived from a lung tumor of a C57BL/6 mice) in the presence and absence of CBX. Since KPTT tumors express cytoplasmic GFP, the fluorescence signal was used as the proliferation readout. KPTT cell proliferation was significantly reduced in the presence of CBX (**Fig 4G, Fig S13B**), indicating the role the of gap junctions in their growth. To test this effect *in vivo*, mice were intubated to generate KP and KPTT genotypes, followed by subcutaneous injection of CBX or vehicle control (NaCl) for 8 weeks. Although no difference was observed in the survival of CBX treated KP mice, the drug significantly delayed the formation of tumors in KPTT mice and increased their mean survival (**Fig 4H**). Compared to vehicle control, most of the KPTT mice either formed no or small tumors (**Fig 4I**). H&E staining of mouse lungs showed that CBX-treated mice developed tumors of comparatively smaller size with visibly intact parenchyma, compared to the larger tumor burden in controls (**Fig S13C**). Taken together, while CBX did not affect the growth of KP tumors, in KPTT mice gap junction inhibition rendered a significant reduction in tumor growth.

Our data presents a strong rational to revisit the canonical notion that synthesis of dTMP in every single transformed cell drives tumor growth and establish a new paradigm of collective proliferation for growth of NSCLC tumors. In the postulated model proliferation can be maintained by dTMP being synthesized in some cells within a tumor and redistributed to other cancer cells via gap junctions (**Fig 5**).

Discussion.

Crosstalk of tumor entities at multiple level is fundamental to cancer growth, such that immunotherapeutic abrogation of receptor driven interaction between cancer cells and immune cells has been one of the major breakthroughs in the clinical intervention of NSCLC and other cancers[30,31]. Metabolic codependency and cross-feeding of metabolites between different tumor entities further adds to this complexity and is equally

important for tumor growth[32,33]. This study advances that concept by identifying dTMP equilibration within tumor as an important growth mechanism and postulates a model of collective proliferation. This has broad implications across tumor pathology, from tumor biology to clinical interventions. Since, proliferation is a fundamental physiological process, the concept of collective proliferation may have a relevance beyond cancer, for instance in proliferative diseases (atherosclerosis, idiopathic pulmonary fibrosis, scleroderma, etc.), embryology and tissue regeneration.

The notion of collective proliferation opens serval follow-up questions, for example, how dTMP deficiency in cancer cells links to activation of gap-junctions and what are the molecular signals that drive their overexpression in dTMP donor cells. Furthermore, it could be of both biological and clinical relevance to understand the fate of senescense in proliferating *TYMS*$^{-}$*TK1*$^{-}$ cells, as it plays critical role in cancer progression and clinical responses[34].

One of the most intriguing observations in this study, that calls for further exploration, is the failure of cells with genetic perturbation causing all-pyrimidines or all-nucleotide deficiency to be restored by coculture, thus restricting the phenomenon of collective proliferation to dTMP sharing. dTMP is certainly distinct as the entity exclusive to deoxyribonucleotide pool, and therefore, might have characteristics that are not shared by other deoxyribonucleotides, which might have important roles in genomic instability and DNA repair during xenobiotic stress.

A major implication of the outcomes relates to therapeutics for NSCLC and other cancers, since targeted metabolic perturbation is central to chemotherapy, including drugs that target TS[11]. In this context, metabolic redistribution by refractory cells might play a critical role in chemoresistance. Collective proliferation might also contribute to resistance against immune therapy where *TYMS*$^{-}$*TK1*$^{-}$ cells might act as nucleotide sponges that affect the differentiation and exhaustion of immune cells[35]. Subsequently, the collective proliferation model may refine therapeutic avenues, for instance by repurposing CBX, which is approved for peptic, esophageal, and oral ulceration[36], or other gap junction inhibitors, for clinical testing of combination therapies. The findings also accentuate the importance of metabolite and resource redistribution in tumors, which might act as an energy-efficient compensatory mechanism for metabolic vulnerabilities[37]. Understanding the origin of *TYMS*$^{-}$*TK1*$^{-}$ during clonal expansion will be a vital addition to proliferation dynamics in

tumor growth. Moreover, because *TYMS*$^{-}$*TK1*$^{-}$ cells were linked to important cancer-associated pathways, the collective proliferation model will prompt novel investigations that unravel fundamental cancer pathology. For example, differential transcriptome of *TYMS*$^{-}$ *TK1*$^{-}$ cells indicates that their proportion might be a functional rheostat for adapting to metabolic heterogeneity[38], overcoming the challenges of harsh growth environment[39] and modulating the dynamics of TME[40].

Another important aspect of dTMP equilibration and collective proliferation is the existence of an intratumoral niche of genetically variant cancer cells (for example between dTMP deficient cells and synthesizing cell), which might involve non-tumor entities, with dedicated metabolic functions important for tumor pathology.

Finally, collective proliferation, particularly in the context of dTMP equilibration, adds another dimension to the metabolic complexity in cancer. Recent advances have attributed moonlighting functions to classical metabolites[41,42]. Such metabolites include pyrimidine metabolites that play a critical role in differentiation[43-47], act as a cofactor in lipogenesis[48], and intercellularly feed glycolysis under metabolic stress[49-51]. This not only repositions the importance of pyrimidine metabolism, which is often considered a terminal outcome of metabolic alterations, but also raises a question of when and how cancer cells decide to metabolize for themselves or supply other cells.

In conclusion, this study repositions proliferation in the context of metabolic resource sharing and establishes a more dynamic and plastic nature of tumor growth. Further exploration of this mechanism will not only enhance the current understanding of the interplay among tumor growth, heterogeneity, and pathology but will also provide a new perspective targeting proliferation.

Acknowledgements. The authors wish to acknowledge the support of Metabolomics Core Facility, EMBL, Heidelberg, Germany for their support with mass-spectrometric quantification, and Dr Thomas Solomon at Blazon Scientific for assistance with drafting the manuscript. Illustrations were drawn using Biorender. The study was funded by Hallas-Møller Ascending Investigator Grant from Novo Nordisk Fonden (PC), Independent Research Fund Denmark (Danmarks Frie Forskningsfond) 0134-00012B (PC), Lundbeck Fonden, Denmark, R380-2021-1264 (MAS, International Association for the Study of Lung Cancer (MAS), Danish Cancer Society (AMAR), Danish Cancer Society (AMT).

Author Contribution. P.C. and M.A.S. were involved in project conceptualization and development and the preparation of the manuscript. P.C., P.S. and M.V. were involved in supervision. M.A.S., A.M.A.R., L.P., S.V., S.S.M., P.N.G. and A.M.T. conducted the experiments. V.R. and N.P.P. conducted the bioinformatic analysis. F.N. was involved in data acquisition.

Declaration of Interests: Authors declare no competing interests.

Resource Availability

Lead contact. Further information and requests for resources and reagents should be directed to and will be fulfilled by the lead contact Paolo Ceppi (pceppi@bmb.sdu.dk).

Materials availability. All the plasmids generated in this study are available from the lead contact without restriction or with a completed materials transfer agreement, which ever applies.

Data and code availability. RNA sequencing data has been deposited to GEO dataset (GSE271721). Any additional information required to reanalyze the data reported in this paper is available from the lead contact upon request

Fig_1

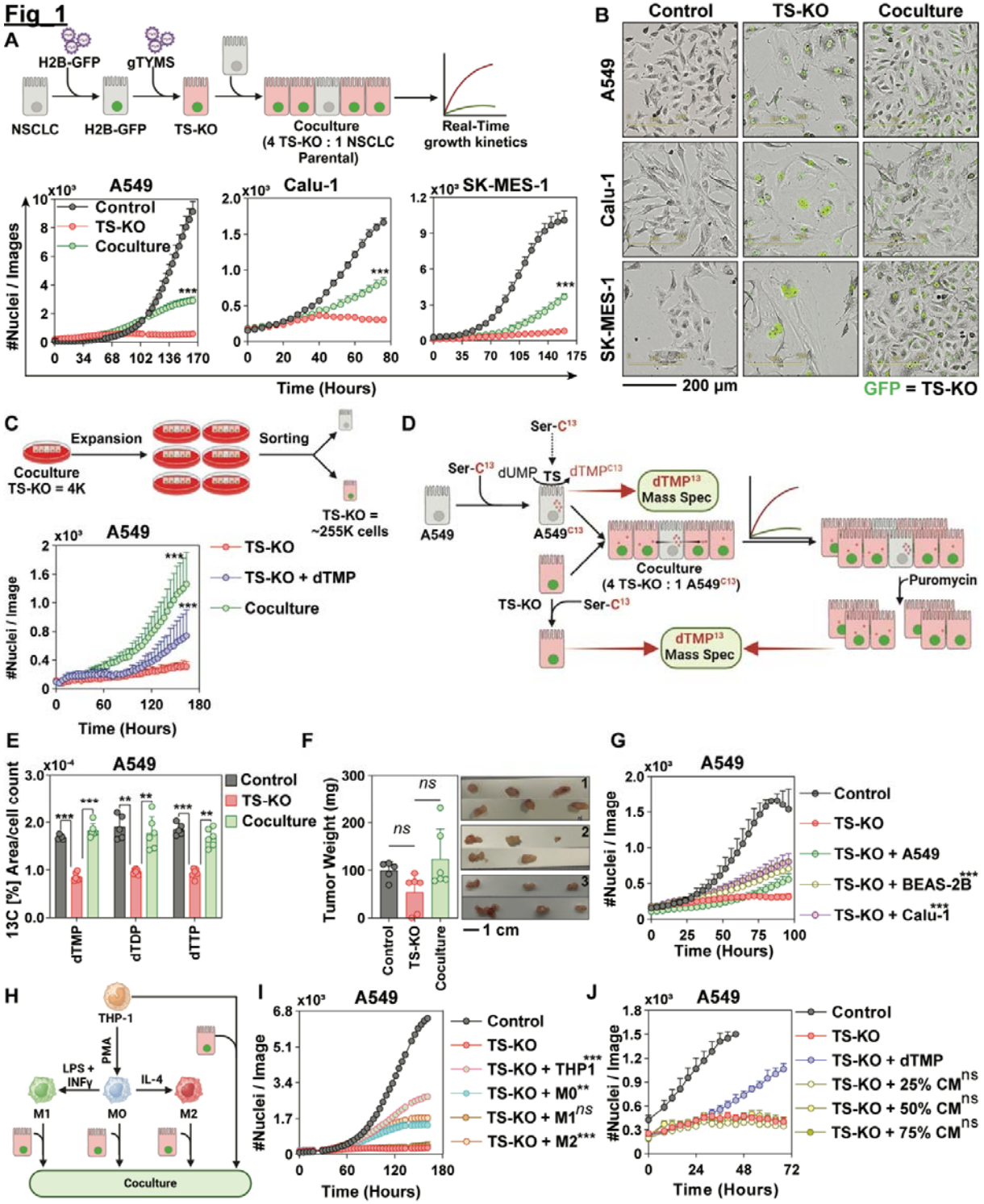
A
H2B-GFP
gTYMS
NSCLC
H2B-GFP
TS-KO
Coculture
(4 TS-KO : 1 NSCLC Parental)
Real-Time growth kinetics
A549
Calu-1
SK-MES-1
Control
TS-KO
Coculture
#Nuclei / Images
Time (Hours)
B
Control
TS-KO
Coculture
A549
Calu-1
SK-MES-1
200 µm
GFP = TS-KO
C
Expansion
Sorting
Coculture
TS-KO = 4K
TS-KO = ~255K cells
A549
TS-KO
TS-KO + dTMP
Coculture
#Nuclei / Image
Time (Hours)
D
Ser-C13
dUMP
TS
dTMP C13
dTMP13 Mass Spec
A549
A549C13
Coculture
(4 TS-KO : 1 A549C13)
TS-KO
Ser-C13
Puromycin
dTMP13 Mass Spec
E
A549
Control
TS-KO
Coculture
13C [%] Area/cell count
dTMP
dTDP
dTTP
F
Tumor Weight (mg)
ns
ns
Control
TS-KO
Coculture
1 cm
G
A549
Control
TS-KO
TS-KO + A549
TS-KO + BEAS-2B
TS-KO + Calu-1
#Nuclei / Image
Time (Hours)
H
THP-1
PMA
LPS + INFγ
IL-4
M1
M0
M2
Coculture
I
A549
Control
TS-KO
TS-KO + THP1
TS-KO + M0
TS-KO + M1
TS-KO + M2
#Nuclei / Image
Time (Hours)
J
A549
Control
TS-KO
TS-KO + dTMP
TS-KO + 25% CM
TS-KO + 50% CM
TS-KO + 75% CM
#Nuclei / Image
Time (Hours)

338

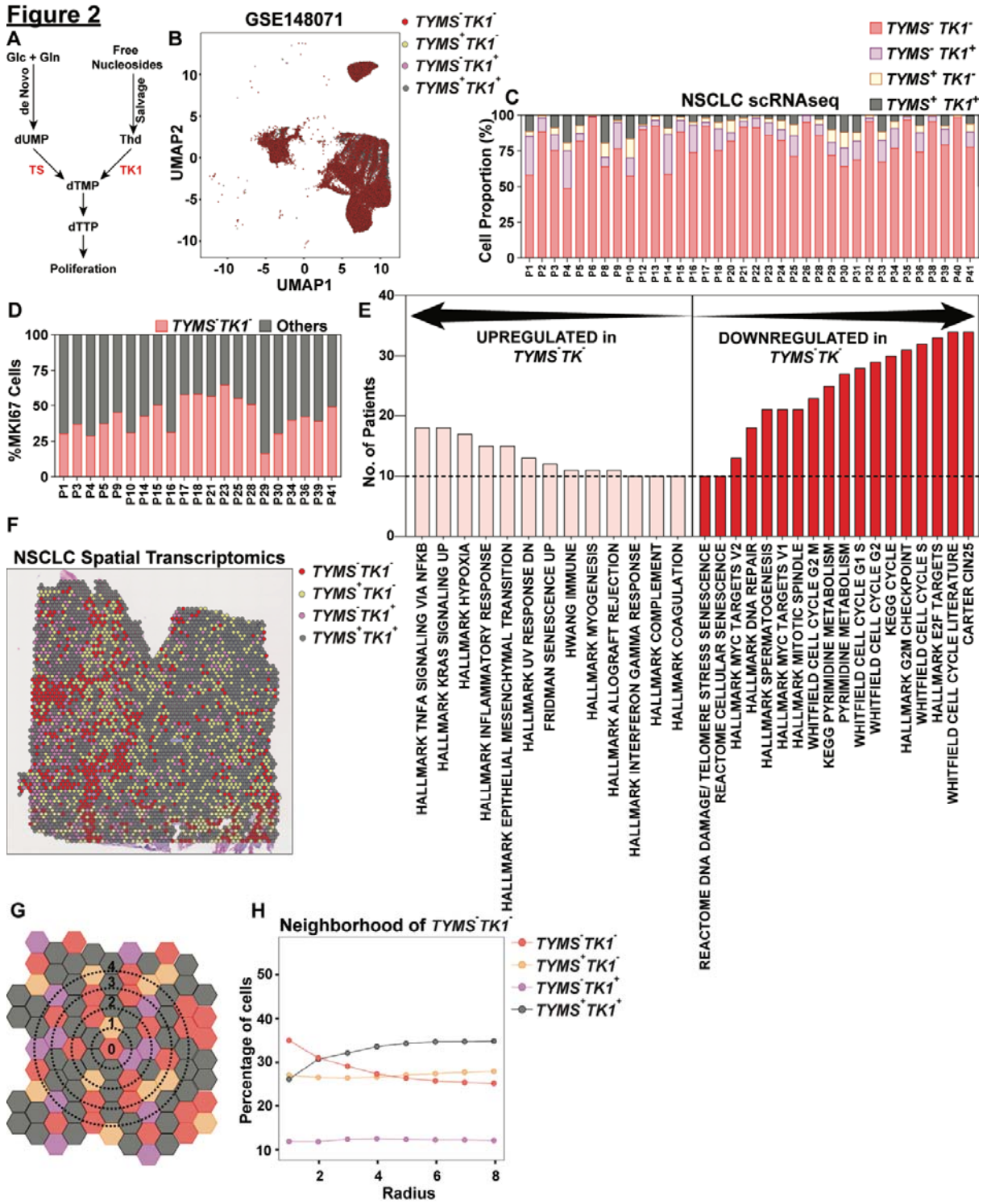
Figure 2
A
Glc + Gln
Free Nucleosides
de Novo
Salvage
dUMP
Thd
TS
TK1
dTMP
dTTP
Poliferation
B
GSE148071
TYMS⁻TK1⁻
TYMS⁺TK1⁻
TYMS⁻TK1⁺
TYMS⁺TK1⁺
UMAP2
UMAP1
C
NSCLC scRNAseq
TYMS⁻ TK1⁻
TYMS⁻ TK1⁺
TYMS⁺ TK1⁻
TYMS⁺ TK1⁺
Cell Proportion (%)
D
TYMS⁻TK1⁻ Others
%MKI67 Cells
E
UPREGULATED in TYMS⁻TK⁻
DOWNREGULATED in TYMS⁻TK⁻
No. of Patients
HALLMARK TNFA SIGNALING VIA NFKB
HALLMARK KRAS SIGNALING UP
HALLMARK HYPOXIA
HALLMARK INFLAMMATORY RESPONSE
HALLMARK EPITHELIAL MESENCHYMAL TRANSITION
HALLMARK UV RESPONSE DN
FRIDMAN SENESCENCE UP
HWANG IMMUNE
HALLMARK MYOGENESIS
HALLMARK ALLOGRAFT REJECTION
HALLMARK INTERFERON GAMMA RESPONSE
HALLMARK COMPLEMENT
HALLMARK COAGULATION
REACTOME DNA DAMAGE/ TELOMERE STRESS SENESCENCE
REACTOME CELLULAR SENESCENCE
HALLMARK MYC TARGETS V2
HALLMARK DNA REPAIR
HALLMARK SPERMATOGENESIS
HALLMARK MYC TARGETS V1
HALLMARK MITOTIC SPINDLE
WHITFIELD CELL CYCLE G2 M
KEGG PYRIMIDINE METABOLISM
PYRIMIDINE METABOLISM
WHITFIELD CELL CYCLE G1 S
WHITFIELD CELL CYCLE G2
KEGG CYCLE
HALLMARK G2M CHECKPOINT
WHITFIELD CELL CYCLE S
HALLMARK E2F TARGETS
WHITFIELD CELL CYCLE LITERATURE
CARTER CIN25
F
NSCLC Spatial Transcriptomics
TYMS⁻TK1⁻
TYMS⁺TK1⁻
TYMS⁻TK1⁺
TYMS⁺TK1⁺
G
H
Neighborhood of TYMS⁻TK1⁻
Percentage of cells
Radius

339

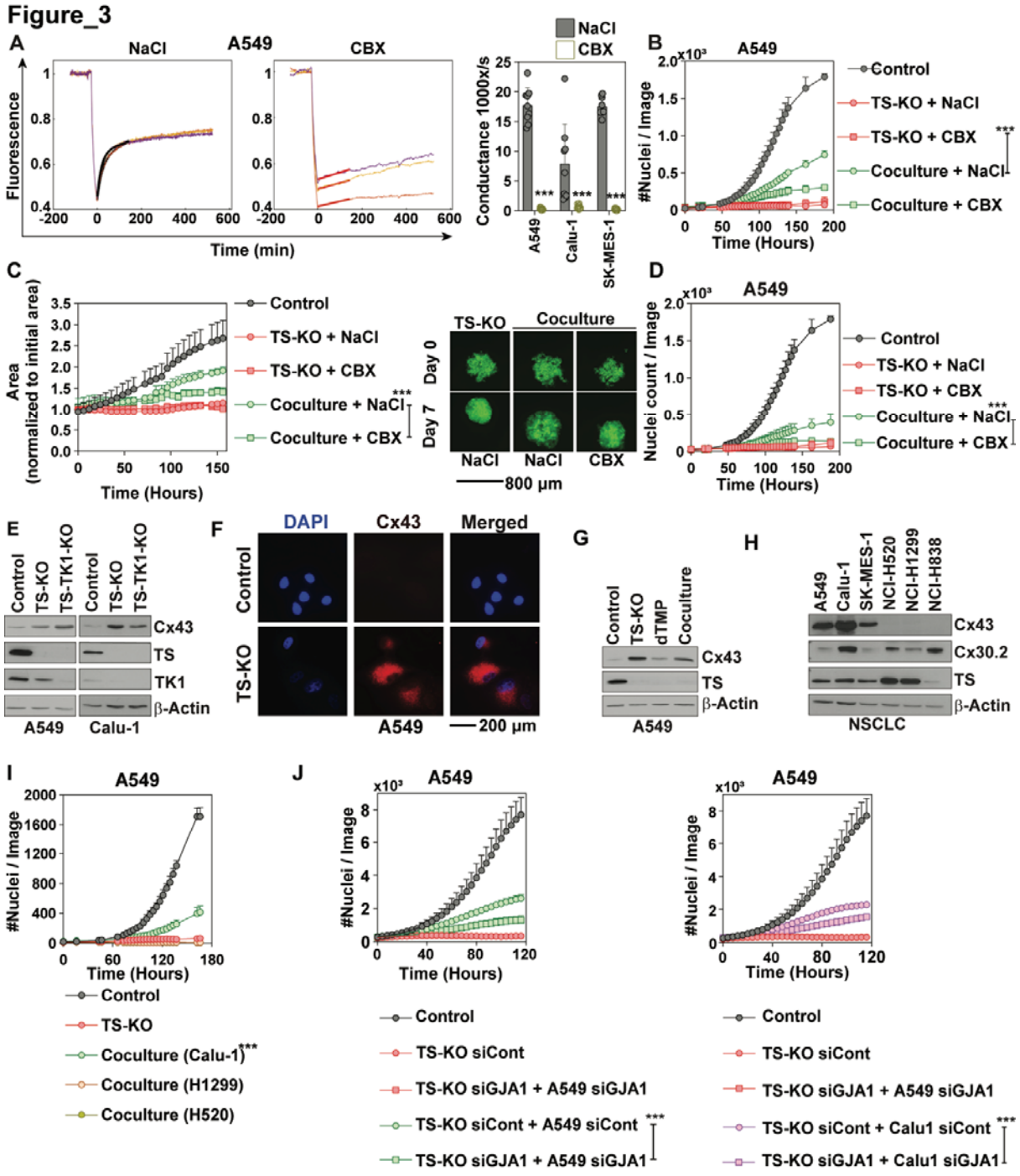
Figure_3
A
NaCl
A549
CBX
Fluorescence
Time (min)
NaCl
CBX
Conductance 1000x/s
A549
Calu-1
SK-MES-1
B
A549
#Nuclei / Image
Time (Hours)
Control
TS-KO + NaCl
TS-KO + CBX
Coculture + NaCl
Coculture + CBX
C
Area (normalized to initial area)
Time (Hours)
Control
TS-KO + NaCl
TS-KO + CBX
Coculture + NaCl
Coculture + CBX
TS-KO
Coculture
Day 0
Day 7
NaCl
NaCl
CBX
800 µm
D
A549
Nuclei count / Image
Time (Hours)
Control
TS-KO + NaCl
TS-KO + CBX
Coculture + NaCl
Coculture + CBX
E
Control
TS-KO
TS-TK1-KO
Control
TS-KO
TS-TK1-KO
Cx43
TS
TK1
β-Actin
A549
Calu-1
F
DAPI
Cx43
Merged
Control
TS-KO
A549
200 µm
G
Control
TS-KO
dTMP
Coculture
Cx43
TS
β-Actin
A549
H
A549
Calu-1
SK-MES-1
NCI-H520
NCI-H1299
NCI-H838
Cx43
Cx30.2
TS
β-Actin
NSCLC
I
A549
#Nuclei / Image
Time (Hours)
Control
TS-KO
Coculture (Calu-1)
Coculture (H1299)
Coculture (H520)
J
A549
#Nuclei / Image
Time (Hours)
Control
TS-KO siCont
TS-KO siGJA1 + A549 siGJA1
TS-KO siCont + A549 siCont
TS-KO siGJA1 + A549 siGJA1
A549
#Nuclei / Image
Time (Hours)
Control
TS-KO siCont
TS-KO siGJA1 + A549 siGJA1
TS-KO siCont + Calu1 siCont
TS-KO siGJA1 + Calu1 siGJA1

340

Fig_4

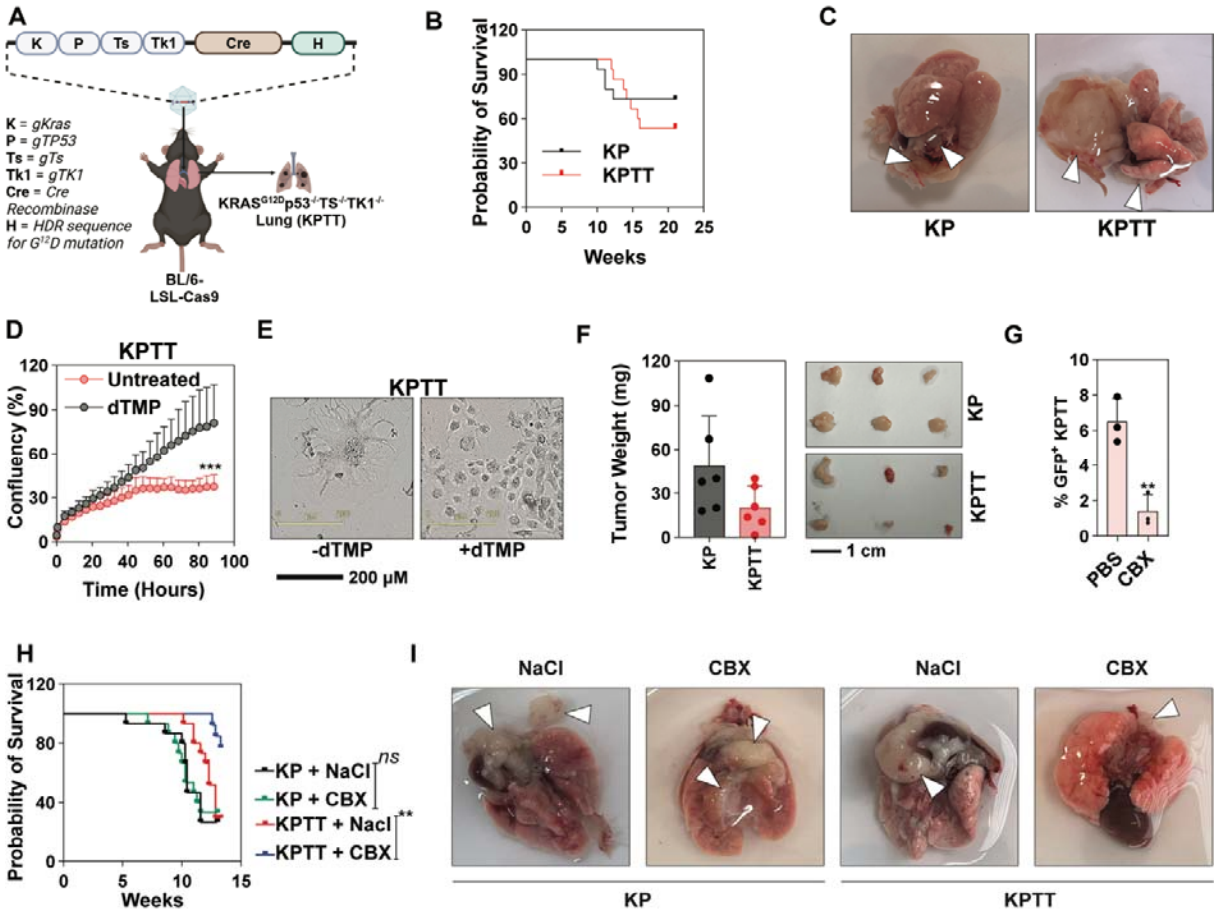
A
K
P
Ts
Tk1
Cre
H
K = gKras
P = gTP53
Ts = gTs
Tk1 = gTK1
Cre = Cre Recombinase
H = HDR sequence for G12D mutation
KRASG12Dp53-/-TS-/-TK1-/-
Lung (KPTT)
BL/6-LSL-Cas9
B
Probability of Survival
Weeks
KP
KPTT
C
KP
KPTT
D
KPTT
Untreated
dTMP
Confluency (%)
Time (Hours)
E
KPTT
-dTMP
+dTMP
200 µM
F
Tumor Weight (mg)
KP
KPTT
1 cm
G
% GFP+ KPTT
PBS
CBX
H
Probability of Survival
Weeks
KP + NaCl
KP + CBX
KPTT + NaCl
KPTT + CBX
ns
I
NaCl
CBX
NaCl
CBX
KP
KPTT

341

Figure_5

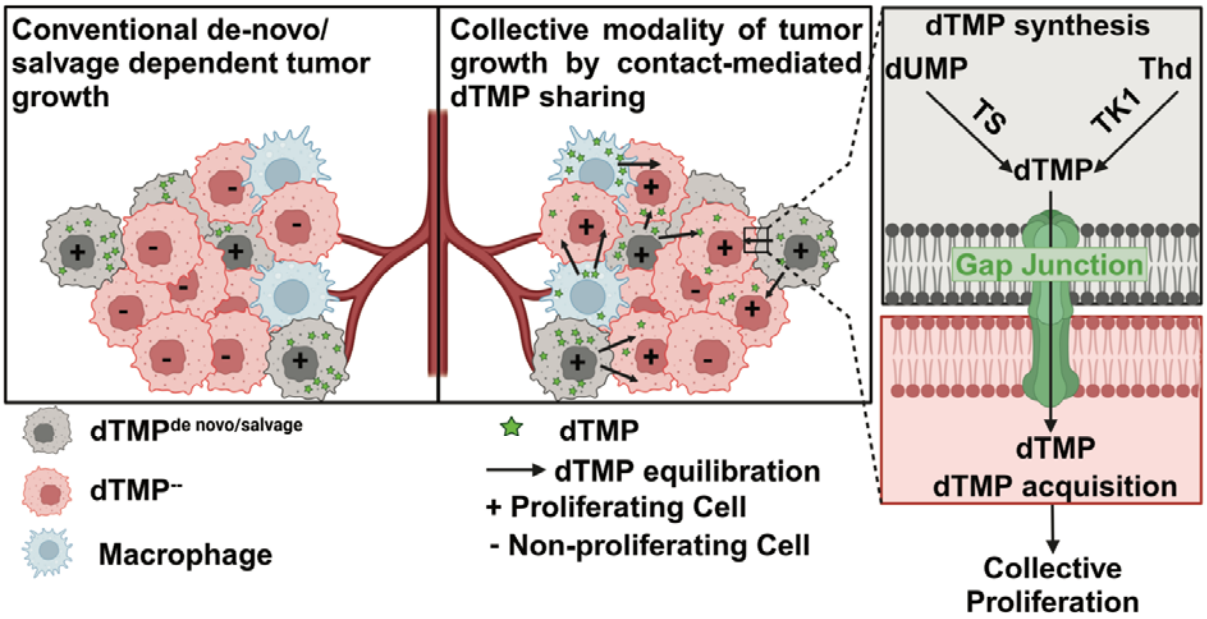

342

343

Figure Titles and Legends

Figure 1. Collective proliferation in NSCLC cancer cells. (A) NSCLC cell lines (A549, Calu-1, SK-MES-1) expressing nuclear H2B-GFP, were knocked out for *TYMS* (pyrimidine de novo gene) by CRISPR/Cas9 and cocultured with their respective parental cells (expressing TS) in a ratio of 4:1. Growth of TS-KO cells was quantified as nuclei counts for GFP^+ cells, by Incucyte S3 real time imager. As experimental controls, GFP-tagged cells were transduced with vector containing a non-targeting sequence. Significance compared to TS-KO cells. The data are mean ± SD of three replicates.

(B) Picture showing morphology of TS-KO cells in coculture, and individual culture compared to their respective controls. TS-KO cells are tagged with H2B-GFP. Images were exported from Incucyte S3 cell imager.

(C) A549 TS-KO cells were cocultured with parental cells for 10 passages, sorted based on GFP expression and reseeded to test their dependency on exogenous dTMP. Cell counts at initial and final passage are indicated. The data are mean ± SD of three replicates.

(D) A549 cells were cocultured in ser C^{13} for 24 hours to enrich the cells for $dTMP^{C13}$ **(**$A549^{C13}$**)**. Puromycin resistant A549 TS-KO cells were cocultured with $A549^{C13}$ and selected with puromycin after their growth. $dTMP^{C13}$, $dTDP^{C13}$ and $dTTP^{C13}$ were quantified in selected KO Cells. $A549^{C13}$ and TS-KO cells enriched with $dTMP^{C13}$ for 24 hours were used as controls.

(E) Quantification of dTMP, dTDP and dTTP tagged with C^{13}. See also the supplementary figure S6. Data are mean ± SD of 6 replicates.

(F) Weights of tumors obtained from subcutaneous injection in NSG mice and their representative pictures. 1= Control, 2 = TS-KO, 3 = Coculture. Data are mean ± SD of 6 tumors.

(G) Coculture setup between A549 TS-KO cells and epithelial cells of non-cancer origin (BEAS2B) and squamous origin (Calu-1). The data are mean ± SD of 3 replicates and the statistical significance is compared to controls of growth of TS-KO cells (red).

(H) Scheme showing differentiation of THP-I monocytes to different lineages. THP-1 cells and cells from derived lineages were cocultured with individually with TS-KO cells.

(**I**) Growth of A549 TS-KO cells in coculture with THP-1 monocytes and their derivatives. The data are mean ± SD of 5 replicates the significance is compared to TS-KO cells.

(J) DMEM was conditioned by A549 cells for 48 hours and then supplemented to growth medium of A549 TS-KO cells and their growth was monitored. The significance is compared to TS-KO and the data are mean ± SD of 6 replicates

Significance test in A, C, G, I and J is Two-Way ANOVA with Tukey's multiple comparison; in E and F is One-Way ANOVA.

Figure 2. Collective proliferation in NSCLC lung cancer patients. **(A)** Scheme showing the canonical de novo and salvage pathways for dTMP synthesis.

(B) Representation of cells with both de novo (TS^+TK1^+), only de novo (TS^+TK1^-), only salvage (TS^-TK1^+) or neither (TS^-TK1^-) from cell types clustered from single cell data for 40 NSCLC patients. Each dot represents a cancer cells. The number of cancer cells is 39,787 out of total 88,672.

(C) Patient-wise distribution of different population from (B). Each bar represents a single patient.

(D) Contribution of $MKI67^+$ proliferative cells in $TYMS^-TK^-$ cells in different patient tumor compared to other populations (TS^+TK1^-, TS^-TK1^+ and TS^+TK1^+), shown only for the patients with at least 50 proliferative cells (Each bar represents a single patient, n = 21).

(D) Pathways that are differentially regulated between TS^-TK1^- and other populations. Only those pathways that were significantly regulated in 10 or more patients are included.

(F) Analysis of spatial transcriptomics data from NSCLC tissue, showing TS^-TK1^- cells distributed throughout the tumor. TS^+TK1^+ = 1763 cells, TS^+TK1^- = 1000 cells, TS^-TK1^+ = 438 cells, TS^-TK1^- = 657 cells.

(G) Schematic representation of neighborhood analysis. Cells surrounding an individual selected cell were assigned a radius depending on its distance (1 to 8). Proportion of TS^+TK1^+, TS^+TK1^-, TS^-TK1^+ and TS^-TK1^- cells was calculated in each radius and radii were averaged to determine percentages of different of cell types.

(H) Neighborhood analysis of TS^-TK1^- cells showing inclusion of more TS^+TK1^+ cells in their surroundings, indicating their tendency to co-exist with TS^+TK1^+. Each point represents the mean of all the neighborhoods.

Figure 3. Gap junctions mediate dTMP sharing and proliferation. (A) FRAP (fluorescence recovery after photobleaching) showing connectivity of indicated cells,

measured by their ability to reconstitute fluorescent dye after bleaching, in presence of either NaCl or 100 µM gap junction inhibitor carbenoxolone (CBX). Each bar represents the mean ± SD of 10 replicates.

(B) Incucyte proliferation assay measuring growth of TS-KO cells in coculture with parental cells in presence of either 100 µM CBX or NaCl. The data are mean ± SD of 3 replicates.

(C) Collective growth of TS-KO cells, as grown in 3D-spheroids, in presence of either 100 µM CBX or NaCl. Images for spheroids showing GFP signal. See also the supplementary figure S11G. Each point represents the mean ± SD of 5 replicates.

(D) Collective growth of TS-KO cells in presence of THP-1 monocytes abrogated by supplementation of 100 µM CBX compared to NaCl. The points is a mean ± SD of 3 replicates.

(E) Increased expression of Cx43 proteins, which hexamerizes to form GJA1 quantified in TS-KO and TS-TK1 KO cells.

(F) Immunofluorescence images showing increase of Cx43 (protein coded by GJA1) in TS-KO cells.

(G) A549 TS-KO cells were allowed to restore proliferation in a coculture with parental cells and were selected by administration of 3 µg/ml of puromycin. Western blot depicts increased expression of GJA1 in TS-KO, where growth has been induced by parental A549. Cells were selected by administration of puromycin after their growth was restored.

(H) NSCLC cell lines classified high and low based on the expression of Cx43.

(I) The ability of high and low cells to promote collective growth in TS-KO cells, as quantified by Incucyte S3. The data are mean ± SD of 3 replicates.

(J) Simultaneous siRNA (80 nM) mediated knockdown of GJA1 in A549 TS-KO and parental cells, and its abrogative effect on collective growth. The data are mean ± SD of 3 replicates.

Significance in (A) is One-Way ANOVA.

Significances in (B, C, D, J) are compared between CBX treatment and NaCl treatment and between TS-KO and others in (I) by Two-Way ANOVA with Tukey's multiple comparison.

Figure 4. Gap junction dependent growth of *TYMS*$^{-}$*TK1*$^{-}$ NSCLC tumors. (A) C57BL/6 expressing Ca9 were intubated with AAV9 vectors carrying gRNA for Kras (along with

G12D HDR sequence), p53, Tyms and TK1 resulting in lung specific mutations in targeted genes. Intubated mice develop $Kras^{G12D}$ and $p53^{-/-}$ driven tumors that lack expression of *Tyms* and *Tk1* genes, resulting in KPTT tumors.

(B) Comparison of tumors formed by mice harboring tumor specific mutation in lungs of C57BL/6 mice. KP ($Kras^{G12D}$ $p53^{-/-}$) mice have been used as controls.

(C) Representative images from lungs with tumors from the mice in (C).

(D) Cell line established from KPTT tumor dependent on exogenous dTMP supplementation for proliferation. The data are mean ± SD of 3 replicates.

(E) Images showing enlarged senescent morphology in absence of dTMP in KPTT cells.

(F) Weight of tumors excised from subcutaneous implantation of KP and KPTT tumors in C57BL/6 along with representative images. Each bar represents the mean ± SD of 6 replicates.

(G) Flowcytometric quantification of GFP^{+} KPTT cells cocultured with syngeneic Ladi 2.1 line derive from lung tumor of a C57BL/6 mouse. Cocultures were treated either with 100 µM CBX or the vehicle control. The bars are mean ± SD of 3 replicates.

(H) Survival of KPTT mice compared to KP mice when treated with 40 mg/kg CBX or corresponding volume of vehicle control NaCl. (n = 15 for all the groups except the KPTT + CBX where n = 14).

(I) Images of lung with tumors for (H). KPTT NaCl lung is from the same week of the representative KPTT + NaCl lung, at the time of the termination of experiment.

Significance in (D) is Two-Way ANOVA with Tukey's multiple comparison, (G) is Student's t-Test and Log-Rank (Mantel Cox) test in (H).

Figure 5. Collective proliferation in tumor growth by dTMP equilibration. The current model of proliferation emphasizes on activation of canonical de novo and/or salvage pathways in each proliferating cell, whereas the model of collective proliferation postulates that growth is a cumulative sum of proliferation of cells with de novo and salvage and cells that rely of dTMP sharing via gap junctions.

Methods

Cell lines. Lung cancer cell lines (A549, Calu-1, SK-MES-1, NCI-H1299, NCI-520, NC-H838) and THP-1 monocytes were purchased from ATCC, and the KPTT cell line was established from C57BL/6 mouse with genetic knock of Ts and Tk1. Normal fibroblasts and

CAFs were provided by Dr. Pamela L. Strissel, at the University Clinic, Erlangen, Germany. Ladi 2.1 cells were obtained from Dr. Markus E. Diefenbacher, Biochemistry and Molecular Biology Biocenter, University of Würzburg, Germany. HEK-293T cells were obtained from Dr. Heiko Wurdak, Faculty of Medicine and Health, School of Medicine, University of Leeds. All cells were cultured in DMEM supplemented with 2 mM of L-glutamine (Gibco), 100 U/ml of Penicillin–Streptomycin (Gibco), and 10% Fetal bovine serum (Gibco), except for THP-1 and Jurkat cells that were cultured in RPMI 1640 (Gibco) supplemented with 10% FBS (Merch) and 1% penicillin-streptomycin (Gibco). All cell lines were kept in culture for no more than 35 passages. All cell lines were authenticated by STR profiling and tested regularly for mycoplasma contamination. Cell lines were maintained at 37°C with 5% CO_2 level in a humidified incubator.

Lentiviral transduction. For the production of lentiviral particles, 293T cells were transfected with 8 µg expression vectors and 2 µg of third-generation lentiviral packaging system in complex with 24µg PEI (Polysciences). After 48 hours, supernatant was collected, centrifuged, and filtered. For transduction, 50,000 cells were seeded in a 6-well plate and transduced with LV-vectors expressing H2B-GFP in presence 32 µg polybrene (Sigma). Cells were sorted for GFP positive cells. To generate stable knockouts, 50,000 cells were transduced with lentiviral particles carrying gRNA for target genes along with CAS9 in presence of 32 µg polybrene. Viruses were removed 24 post the transduction, whereas selection was started 48 post transductions. TS-KO cells and TS-TK1-KO cells were selected with 3 µg/ml puromycin (Sigma). Cells transfected with gRNA for TK1, DTYMK, and RRM1 were selected with 1 mg /ml hygromycin (Sigma). Plasmids have been listed as Table S1.

Metabolite treatments. For metabolite treatments, cells were seeded at a density of 1800–2000 cells/well in a 96-well plate. Medium was changed on the following day and cells were then treated with metabolites. The plates were imaged in Incucyte S3 and proliferation was recorded as the number of green nuclei.

THP-1 differentiation. THP-1 monocytes were differentiated into macrophages by stimulation with phorbol 12-myristate 13-acetate (PMA). Briefly, 800.000 THP-1 cells were stimulated with 100 ng/ml PMA for two days in a 6-well plate. During the stimulation the THP-1 cells would adhere to the surface of the well. To further differentiate the

macrophages into M1- or M2 macrophages the cells were stimulated with 100 ng/ml lipopolysaccharide (LPS) (Sigma-Aldrich) and 20 ng/ml interferon gamma (IFNγ) (Peprotech) or 20 ng/ml interleukin 4 (IL4) (Peprotech) respectively for 72 hours. During the M1- and M2 polarization, M0 macrophages were cultured in RPMI supplemented with 10% FBS and 1% P/S.

Coculture experiments. For coculture experiments, 1800–2000 H2B-GFP-TS-KO (or TSTK1-KO cells) cells were seeded with dTMP donor cells in 96-well plates. Coculture was optimized by trying different ratios between TS-KO and the dTMP donor cells. For coculture with A549, Calu-1, SK-MES-1, BEAS2B, NCI-H1299, NCI-H838 and NCI-520 ratio of 1:4 was used. Jurkat cells were stimulated with CD3/CD28 dynabeads (Gibco) according to the manufacture's protocol and 30 U/ml interleukin-2 (IL-2) (Gibco) during the duration of the coculture. The proliferation of the H2B-expressing cells was monitored using IncuCyte S3 (Sartorius). The plates were scanned every 4-8 h. For each scan, phase contrast and fluorescence images were acquired from every well. Images were analyzed using IncuCyte S3 software to obtain the number of GFP^+ nuclei.

Tumor-educated macrophages. Tumor-educated macrophages (TEM) were made based on the protocol describe earlier (*14*). Initially, 1.5 million A549 cells were cultured in DMEM supplemented with 10% FBS, 1% P/S, and 1% L-glutamine in a 10-cm dish. One day after seeding, the medium was changed on the 50% confluent A549 cells, and the cells were cultured for an additional 48 hours. Next, the conditioned medium was collected from the A549 cells and centrifuged at 300 × g for 5 minutes. The conditioned medium was then filtered through a 0.45 um filter and heat-inactivated for 15 minutes at 100°C. DMEM supplemented with 10% FBS, 1% P/S, and 1% L-glutamine was added to the conditioned medium to restore the initial volume. Similar to the *THP-1 differentiation* described above, 1.6 million THP-1 cells per well of a 6-well plate were stimulated with 100 ng/ml PMA for 48 hours, then the medium was removed and replaced with 75% heat-inactivated conditioned medium from the A549 cells. The THP-1 cells were cultured for an additional 48 hours to polarize them into TEM. Then then conditioned medium from the TEM was collected, centrifuged at 300 × g for 5 minutes, and heat-inactivated at 100°C for 15 minutes. Different percentages of conditioned medium were added to 1.800 A549 H2B.GFP TS-KO cells in a 96-well plate as specified in the figure legends. The TEM

macrophages were collected by trypsination and cocultured with A549 H2B.GFP TS-KO cells cells in different ratios as described above in *Coculture experiments*.

Transwell cocultures. 0.4 µm pore polyester membrane transwells (Corning) were used for transwell cocultures. 2000arental A549 cells were seeded on the upper chamber and the 8000 TS-KO cells were seeded on the lower chamber. The growth of TS-KO cells was monitored by Incucyte S3.

Drug Treatments. Carbenoxolone (CBX, Sigma) and SMIFH2 (Tocris) were first titred in cells to determine the non-toxic concentration. For cocultures, 60,000 parental cells and TS-KO cells were seeded in the determined concentration of the drugs (100 µM CBX and 50 µM SMIFH2), along with the respective vehicle controls (0.1 % ,NaCl for CBX, 0.1 %DMSO for SMIFH2). Coculture was set up on the following day with the pretreated cells in the presence of either the drug or the control.

Spheroid Coculture. 2000 TS-KO cells per well were seeded in the presence or absence of coculture with parental cells in 100 µM CBX and 0,1 % NaCl in a 96-well ultra-low attachment plate. The plate was centrifuged at 300 rpm for 10 min at 20°C and then incubated at 37°C for 3 days until the spheroids attained a desired diameter of 200–500 µm. The spheroids were then re-treated with CBX (100 µM) or with 0.1% NaCl. Next, the plate was pre-cooled on ice, matrigel matrix was added to the spheroids, and the plate was centrifuged at 300 rpm for 5 min at 4°C. Then, the matrigel was polymerized in an incubator at 37°C for 30 min. The spheroids were then monitored and the brightfield and green area of the spheroids were measured using a real-time spheroid invasion assay every 4 h for 5 days in Incucyte S3.

Western Blot. For western blots, 5–20 µg of protein were resolved on 12% bis-acrylamide gel and transferred on 0.45 µm PVDF membrane (Thermo). Membranes were blocked in 5% milk (Biorad) in 1X TBS-T (1% Tween20 in Tris Buffer Saline) and incubated with primary antibody overnight at 4°C. Post incubation, membranes were washed with 1X TBS-T and incubated with HRP-conjugated secondary antibody for an hour at room temperature. ECL substrate was then added to the membrane and the bands were recorded on X-RAY films (Thermo) and developed and fixed manually. A list of antibodies and dilutions is provided in Table S2.

β-Galactosidase staining. A Senescence β-Galactosidase Staining Kit from Cell Signaling Technology was used. In brief, cells were seeded to a low confluence in a 6- or 12-well plate. 24 hours after the seeding medium was changed, cells were fixed and stained following the instructions from the manufacturer. Stained cells were visualized and imaged using an Olympus BX53 microscope. Positive cells and total cells were counted using ImageJ and positively stained cells were normalized to the total number of cells.

siRNA transfection. Reverse transfection was done with Lipofectamine RNAiMAX Transfection Reagent (Thermo). The transfection complex was prepared by adding 80 nM siRNA to 2 µl transfection reagent in 200 µl serum free DMEM and incubated for 15 minutes. After incubation, the transfection complex was added to the bottom of 12-well plates, 60,000 cells per well were suspended in 800 µl, and cells were incubated at 37°C in 5% CO_2. 24 hours post transfection, cells were used to establish cocultures. Knock down was confirmed in the lysates that were collected 48 hours after the transfection.

Immunofluorescence. For immunofluorescence, 100,000 cells were seeded in 6-well plates on coverslips. For coculture conditions, H2B-GFP KO cells were seeded with non-GFP/RFP parental cells. A day after the seeding, cells were fixed with 4% formaldehyde for 5 minutes followed by 10 minutes of permeabilization with PBS-T (0.1% Triton-X100 in 1X PBS). Cells were blocked in 3% blocking buffer (3% BSA in PBS-T) and incubated in antiGJA1 antibody (diluted 1:200 in blocking buffer) overnight at 4°C. Then, cells were washed with 1X-PBS and incubated with secondary antibody conjugated with Alexa-488 (diluted 1:250 in blocking buffer) for an hour. Cells were then mounted in DAPI containing mounting medium and visualized using an Olympus BX53 microscope.

FRAP for measuring coupling. Monolayers in 4-well ibidi imaging slides were loaded with calcein red-orange (Invitrogen, F10319) for 10 min in HEPES RPMI. Medium was then replaced by fresh medium to remove unloaded dye. Confluent monolayers were imaged using a Zeiss LSM 700 confocal microscope. A cell in the middle of a confluent cluster was selected for bleaching (high-power 555 nm) until fluorescence at 555 nm excitation and emission >590 nm decreased by 50%. The fluorescence signal was measured in the central cell, neighboring cells, and more remote cells, and normalized to the initial intensity. Recovery was fitted to a monoexponential to calculate calcein permeability (in µm/min) from the product of the geometric perimeter and the area of the

central cell, divided by the time constant of fluorescence recovery. Permeability from FRAP recording was calculated as described previously (*10*).

***In vitro* quantification of C13 thymidylate.** For dTMP13 quantification in KO cells, A549 parental cells (puromycin sensitive) were seeded at a density of 2,000,000. After 24 hours medium was replaced with medium supplemented with 400 µM 1-^{13}C-Serine (Sigma). After 24 hours of C13 enrichment, 1,000,000 A549 KO cells were seeded with C13 enriched parental cells. Cell growth was monitored using Incucyte and after the growth of KO cells was restored, 10 µg/ml puromycin was added to the culture to eliminate the puromycin sensitive parental cells. After the parental cells were cleared form the culture, KO cells were washed 5 times with 1X PBS and then 1 ml of prechilled extraction solution was added (Methol:Isonitrile:Water; 2:2:1). Cells were incubated on dry ice for 20 minutes and then scraped and collected in 2 ml Eppendorf tubes. After further homogenization on dry ice via a bead beater (FastPrep-24; MP Biomedicals, CA, USA) at 6.0 m/s (3 x 30 s, 5 min pause time) using 1.0 mm zirconia/glass beads (Biospec Products), samples were centrifuged at 15,000 × g and 4 °C for 10 minutes using a 5415R microcentrifuge (Eppendorf) and supernatants were transferred. The remaining pellet was reextracted by addition of 500 µL of a mixture of H2O:MeOH:ACN (1:2:2, v/v) and bead beating (see conditions described above). After centrifugation, supernatants of corresponding samples were combined and dried under a stream of nitrogen (Organomation Microvap). Dried samples were reconstituted in 50 µL H2O:MeOH:ACN (1:2:2, v/v), vortexed, centrifuged, and transferred to an analytical glass vials. The LC-MS/MS analysis was initiated within one hour after the completion of the sample preparation.

LC-MS/MS analysis. LC-MS/MS analysis was performed on a Vanquish UHPLC system coupled to an Orbitrap Exploris 240 high-resolution mass spectrometer (Thermo) in positive ESI (electrospray ionization) mode. Chromatographic separation was carried out on an Atlantis Premier BEH Z-HILIC column (Waters; 2.1 mm x 100 mm, 1.7 µm) at a flow rate of 0.25 mL/min. The mobile phase consisted of water:acetonitrile (9:1, v/v; mobile phase phase A) and acetonitrile:water (9:1, v/v; mobile phase B), which were modified with a total buffer concentration of 10 mM ammonium acetate. The aqueous portion of each mobile phase was adjusted to pH 9.0 via addition of acetic acid. The following gradient (20 min total run time including re-equilibration) was applied (time [min]/%B): 0/95, 2/95, 14.5/60, 16/60, 16.5/95, 20/95. Column temperature was maintained at 40°C, the

autosampler was set to 4°C and sample injection volume was set to 5 µL. dTMP isotopologues were recorded via a targeted selected ion monitoring (tSIM) scan with a mass resolving power of 120,000 over a 5 Da isolation window set to m/z = 322.5 (scan time: 150 ms, RF lens: 70%). Ion source parameters were set to the following values: spray voltage: -3500 V, sheath gas: 30 psi, auxiliary gas: 5 psi, sweep gas: 0 psi, ion transfer tube temperature: 350°C, vaporizer temperature: 300°C.

All experimental samples were measured in a randomized manner. Pooled quality control (QC) samples were prepared by mixing equal aliquots from each processed sample. Multiple QCs were injected at the beginning of the analysis in order to equilibrate the analytical system. A QC sample was analyzed after every 5th experimental sample to monitor instrument performance throughout the sequence. For determination of background signals and subsequent background subtraction, an additional processed blank sample was recorded. Data was processed using TraceFinder 5.1 and raw peak area data was exported for relative metabolite quantification.

Cell-line derived xenografts. For cell line derived xenografts, cells were counted, and 500,000 cells were suspended in 40 µl Matrigel (Corning)/1X PBS (1:1). Cells were subcutaneously injected in mice in the flanks NSG (NOD scid gamma) mice. Once palpable tumors were observed, mice were sacrificed, by cervical dislocation and umors were extracted and weighed. Mouse experiments were approved by The Danish Animal Experiments Inspectorate at Dyreforsoegstilsynet (License Number 2020-15-0201-00691).

CRISPR/Cas9-mediated lung tumorigenesis. Ultra-purified recombinant adeno-associated virus carrying gRNA for Kras-p53 (AAV-KP) and Kras-p53-Ts-Tk1 (KPTT) was produced and obtained from VectorBuilder Inc., USA. The mice were randomized for age (8–40 weeks) and a viral titer of 3×10^{11} was delivered via an oropharyngeal route to the lungs of C57BL/6 mice with cre-controlled expression of Cas9 (B6J.129(B6N)-Gt(ROSA)$^{26Sortm1(CAG_cas9*,_EGFP)Fezh/J}$). gender, resulting in two mouse genotypes: B/6.Kras$^{G12D/G12D}$p53$^{\Delta/\Delta}$ (KP) and B/6.Kras$^{G12D/G12D}$p53$^{\Delta/\Delta}$Ts$^{\Delta/\Delta}$Tk1$^{\Delta/\Delta}$ (KPTT). Mice were weighed weekly and sacrificed when they showed signs of asphyxiation and a 20% drop in body weight. Lungs were then collected and fixed in 4% buffered formalin and stained for H&E. For CBX treatment, KP and KPTT mice were subjected to biweekly treatment of 40 mg/kg CBX or corresponding dose of 0.9% NaCl and breathing patterns

and bodyweight were monitored. Mouse experiments were approved by The Danish Animal Experiments Inspectorate at Dyreforsoegstilsynet. License Number 2020-15-0201-00607.

Flow Cytometry and Sorting. For counting GFP^+ KPTT cells, cells were trypsinized, resuspended in PBS, run through a FACS Aria-III flow cytometer, and GFP+ cells were gated on the FITC channel. Flow data was analyzed on FlowJo. For FACS of A549 TS-KO cells in coculture, cells were trypsinized and resuspended in PBS, and GFP^+ TS-KO cells were gated using non-GFP parental controls. Sorted TS-KO and Parental cells were reseeded for cocultures and monitored in Incucyte for proliferation.

RNA-sequencing. Total RNA was isolated as per the manufacturer's protocol (Qiazol) from the A549 parental cell line and A549 *TYMS*-knockout and coculture conditions. Similarly, total RNA was isolated from lung tumor tissues of KP and KP-TT (*TYMS* and *TK1* double knockout) mice. 500 ng of total RNA was then diluted in 25 µl of nuclease-free water to construct the sequencing libraries using a NEBNext Ultra RNA Library Prep Kit for Illumina followed by paired-end sequencing using a NovaSeq 6000 platform (Illumina), as described by the manufacturer's protocol. Fastq files generated from sequencing were subjected to quality control analysis using FastQC package. Alignment of the reads to the human reference genome (GRCh38 release 105) along with the respective human gene annotation file was performed using STAR aligner v2.7.9a. The GRCm39 release 108 was used as the reference genome for mouse genome alignment. After the alignment, the reads were counted using the Featurecounts function in the Rsubread v2.10.5 package in R 4.2.1 and subjected to differential gene expression analysis using the DESeq2 v1.36.0 package in R with an adjusted p-value<0.001 and fold change of 2.

Single-cell RNA-sequencing. Single-cell RNA-sequencing data of tumors from lung cancer patients were obtained from the public repository Gene Expression Omnibus (GSE148071, N = 42). The analysis was performed as described previously (*18*). In brief, the obtained raw data was subjected for quality control analysis, and removed cells with number of genes expressed < 200 & > 5000, UMIs with > 30,000 number of molecules and > 30% of mitochondrial content. The filtering of cells was performed for each patient's sample and also in a pooled manner. Two patient samples (patient 19 and patient 27) were excluded from the analysis as the raw data contained duplicate gene names. Seurat v4.2.1

was used to normalize the counts for the library size and identified 600 variable genes to scale the data for principal component analysis (PCA). Cell clusters were identified with the first 20 principal components from PCA and using a Lovain algorithm with a resolution set to 1.0. The identified cell clusters were visualized using uniform manifold approximation and the projection (UMAP) dimensionality reduction method. Cell clusters were scored and assigned to one of 11 major cell types based on the manual inspection of the cell type markers' normalized expression level in UMAP and also with the differentially expressed genes level using the FindAllMarkers function in Seurat. The highest scored cell type was assigned to each cluster. Markers used for the cell type assignment were: Endothelial cells (*CLDN5*, *VWF* and *PECAM1*), Fibroblasts (*COL1A1*, *COL1A2* and *DCN*), Neutrophils (*CSF3R*, *S100A8* and *S100A9*), Mast cells (*GATA2*, *TPSAB1* and *TPSB2*), Alveolar cells (*CLDN18*, *AQP4* and *FOLR1*), T cells (*CD2*, *CD3D*, *CD3E* and *CD3G*), Epithelial cells (*CAPS* and *SNTN*), Myeloid (*CD14* and *LYZ*), B cells (*CD79A* and *CD79B*) and follicular dendritic cells (*FDCSP*).

Cancer cell clusters were assigned with *EPCAM*-positive gene expression and negative for normal lung epithelial makers. We did not find cancer cell clusters in 4 patient samples (patient 7, patient 11, patient 37 and patient 42). In the subsequent analysis, cell clusters assigned with the same cell type were pooled together. The number of cells in each cell type per patient is provided in the Supplementary Data S1. Next, cancer cell clusters were filtered to categorize each cancer cell based on *TYMS* and *TK1* expression levels. In brief, cells were assigned as follows: normalized expressions of *TYMS* > 0 and *TK1* = 0 as $TYMS^{+}TK1^{-}$, *TYMS* = 0 and *TK1* > 0 as $TYMS^{-}TK1^{+}$, *TYMS* > 0 and *TK1* > 0 as $TYMS^{+}TK1^{+}$, and finally *TYMS* = 0 and *TK1* = 0 as $TYMS^{-}TK1^{-}$. The number of cells in each of the categorized cell sub-types based on *TYMS* and *TK1* expression for each patient is provided in Supplementary Data S2.

With the assigned *TYMS* and *TK1* expression status for the cancer clusters, gene set enrichment analysis (GSEA) was performed utilizing the hallmark gene sets and other gene sets related to senescence and pyrimidine metabolism collected from MSigDB v2023.2.Hs and gene sets for chromosomal instability and immune response from previous reports (*44-46*). The details of the gene sets are provided in the Supplementary Data S3. A ranked gene list based on a log2 fold change was generated using FindMarkers function by comparing the $TYMS^{-}TK1^{-}$ to rest of the cell status ($TYMS^{+}TK1^{-}$,

TYMS^{-}*TK1*$^{+}$ and *TYMS*$^{+}$*TK1*$^{+}$). GSEA was performed using fgsea package in R for the rank ordered gene list with the obtained gene sets in each patient sample. Significant gene sets were filtered with a p-value < 0.05 and the number of occurrences of each gene set across patient samples (N = 36) were tabulated. With a threshold of more than 10 patient samples, the gene sets were considered to be either enriched or diminished in *TYMS*$^{-}$*TK1*$^{-}$ cells compared to the other cell states (*TYMS*$^{+}$*TK1*$^{-}$, *TYMS*$^{-}$*TK1*$^{+}$ and *TYMS*$^{+}$*TK1*$^{+}$). A detailed list of enriched gene sets in each patient sample is provided in Supplementary Data S4. In case of proliferative marker analysis, cancer cells positive for *MKI67* marker (*MKI67* > 0) were filtered and analyzed for the proportion of different cell states based on *TYMS* and *TK1* expression levels. The number of each cell subtype status in the *MKI67* subset population is listed in Supplementary Data S5.

Neighborhood analysis of Visium spatial sequencing. Spatial data was downloaded from X10 genomics (https://www.10xgenomics.com/datasets/human-lung-cancer-ffpe-2-standard). Sample id CytAssist_FFPE_Human_Lung_Squamous_Cell_Carcinoma. Spatial coordinates for Visium spots were extracted from the Seurat object and each spot was annotated with their transcription phenotype as TYMS positive, TK1 positive, double positive, or double negative depending on the expression of TYMS and TK1 genes. For every spot, the phenotypes of neighboring spots within a specified radius were counted using a fixed radius nearest neighbor method using the R dbscan package (*47*). Then for each phenotype, the mean number of neighbors was calculated across all spots expressing that phenotype. The neighborhood analysis was repeated for increasing radii (from 1 to 10) where the number of neighbors surrounding a given spot is calculated as Σ6n where n is the radius. Note that only those spots with complete neighbors (i.e. the number of neighbors must be equal to Σ6n, which is not the case with spots closer to the slide boundaries) were used for calculating the mean number of neighbors by phenotype; this was subsequently plotted as a percentage of cells of each phenotype surrounding a cell of given phenotype. Analysis was done in R v4.4 a.

Statistical analysis

All statistical analyses were performed using GraphPad Prism 8.3.0, unless stated otherwise. Comparison-groups are indicated either in the figures with lines or stated in the

figure legends. P-values of statistical significance are illustrated as follows: *<0.05; **p<0.01; ***p<0.001; ****p<0.0001, ns represents non-significant results.

References

1. Ma, J., Zhong, M., Xiong, Y., Gao, Z., Wu, Z., Liu, Y., and Hong, X. (2021). Emerging roles of nucleotide metabolism in cancer development: progress and prospect. Aging (Albany NY) *13*, 13349-13358. 10.18632/aging.202962.
2. Kollareddy, M., Dimitrova, E., Vallabhaneni, K.C., Chan, A., Le, T., Chauhan, K.M., Carrero, Z.I., Ramakrishnan, G., Watabe, K., Haupt, Y., et al. (2015). Regulation of nucleotide metabolism by mutant p53 contributes to its gain-of-function activities. Nat Commun *6*, 7389. 10.1038/ncomms8389.
3. Santana-Codina, N., Roeth, A.A., Zhang, Y., Yang, A., Mashadova, O., Asara, J.M., Wang, X., Bronson, R.T., Lyssiotis, C.A., Ying, H., and Kimmelman, A.C. (2018). Oncogenic KRAS supports pancreatic cancer through regulation of nucleotide synthesis. Nature Communications *9*, 4945. 10.1038/s41467-018-07472-8.
4. Ali, E.S., Sahu, U., Villa, E., O'Hara, B.P., Gao, P., Beaudet, C., Wood, A.W., Asara, J.M., and Ben-Sahra, I. (2020). ERK2 Phosphorylates PFAS to Mediate Posttranslational Control of De Novo Purine Synthesis. Molecular Cell *78*, 1178-1191.e1176. https://doi.org/10.1016/j.molcel.2020.05.001.
5. Kim, J., Hu, Z., Cai, L., Li, K., Choi, E., Faubert, B., Bezwada, D., Rodriguez-Canales, J., Villalobos, P., Lin, Y.F., et al. (2019). Author Correction: CPS1 maintains pyrimidine pools and DNA synthesis in KRAS/LKB1-mutant lung cancer cells. Nature *569*, E4. 10.1038/s41586-019-1133-3.
6. Tardito, S., Oudin, A., Ahmed, S.U., Fack, F., Keunen, O., Zheng, L., Miletic, H., Sakariassen, P.Ø., Weinstock, A., Wagner, A., et al. (2015). Glutamine synthetase activity fuels nucleotide biosynthesis and supports growth of glutamine-restricted glioblastoma. Nature Cell Biology *17*, 1556-1568. 10.1038/ncb3272.
7. Gonzalez Herrera, K.N., Zaganjor, E., Ishikawa, Y., Spinelli, J.B., Yoon, H., Lin, J.-R., Satterstrom, F.K., Ringel, A., Mulei, S., Souza, A., et al. (2018). Small-Molecule Screen Identifies De Novo Nucleotide Synthesis as a Vulnerability of Cells Lacking SIRT3. Cell Reports *22*, 1945-1955. https://doi.org/10.1016/j.celrep.2018.01.076.
8. Mullen, N.J., and Singh, P.K. (2023). Nucleotide metabolism: a pan-cancer metabolic dependency. Nature Reviews Cancer *23*, 275-294. 10.1038/s41568-023-00557-7.
9. Burrell, R.A., McGranahan, N., Bartek, J., and Swanton, C. (2013). The causes and consequences of genetic heterogeneity in cancer evolution. Nature *501*, 338-345. 10.1038/nature12625.
10. Monterisi, S., Michl, J., Hulikova, A., Koth, J., Bridges, E.M., Hill, A.E., Abdullayeva, G., Bodmer, W.F., and Swietach, P. (2022). Solute exchange through gap junctions lessens the adverse effects of inactivating mutations in metabolite-handling genes. Elife *11*. 10.7554/eLife.78425.
11. Wilson, P.M., Danenberg, P.V., Johnston, P.G., Lenz, H.J., and Ladner, R.D. (2014). Standing the test of time: targeting thymidylate biosynthesis in cancer therapy. Nat Rev Clin Oncol *11*, 282-298. 10.1038/nrclinonc.2014.51.

12. Monica, V., Scagliotti, G.V., Ceppi, P., Righi, L., Cambieri, A., Lo Iacono, M., Saviozzi, S., Volante, M., Novello, S., and Papotti, M. (2009). Differential Thymidylate Synthase Expression in Different Variants of Large-Cell Carcinoma of the Lung. Clinical Cancer Research *15*, 7547-7552. 10.1158/1078-0432.Ccr-09-1641.
13. Ceppi, P., Volante, M., Saviozzi, S., Rapa, I., Novello, S., Cambieri, A., Lo Iacono, M., Cappia, S., Papotti, M., and Scagliotti, G.V. (2006). Squamous cell carcinoma of the lung compared with other histotypes shows higher messenger RNA and protein levels for thymidylate synthase. Cancer *107*, 1589-1596. https://doi.org/10.1002/cncr.22208.
14. Diehl, F.F., Miettinen, T.P., Elbashir, R., Nabel, C.S., Darnell, A.M., Do, B.T., Manalis, S.R., Lewis, C.A., and Vander Heiden, M.G. (2022). Nucleotide imbalance decouples cell growth from cell proliferation. Nature Cell Biology *24*, 1252-1264. 10.1038/s41556-022-00965-1.
15. Gehring, H., and Schröder, A. (1991). Thymidine secretion by cultured chicken embryo fibroblasts and NIH/3T3 cells: quantification and time course. Biochem Biophys Res Commun *177*, 259-264. 10.1016/0006-291x(91)91976-j.
16. Fukasawa, M., Bryant, S.M., and diZerega, G.S. (1988). Incorporation of thymidine by fibroblasts: Evidence for complex regulation by postsurgical macrophages. Journal of Surgical Research *45*, 460-466. https://doi.org/10.1016/0022-4804(88)90196-5.
17. Orita, H., Campeau, J.D., Nakamura, R.M., and diZerega, G.S. (1986). Modulation of fibroblast proliferation and transformation by activated macrophages during postoperative peritoneal reepithelialization. American Journal of Obstetrics and Gynecology *155*, 905-911. https://doi.org/10.1016/S0002-9378(86)80048-5.
18. Halbrook, C.J., Pontious, C., Kovalenko, I., Lapienyte, L., Dreyer, S., Lee, H.J., Thurston, G., Zhang, Y., Lazarus, J., Sajjakulnukit, P., et al. (2019). Macrophage-Released Pyrimidines Inhibit Gemcitabine Therapy in Pancreatic Cancer. Cell Metab *29*, 1390-1399.e1396. 10.1016/j.cmet.2019.02.001.
19. Bitter, E.E., Townsend, M.H., Erickson, R., Allen, C., and O'Neill, K.L. (2020). Thymidine kinase 1 through the ages: a comprehensive review. Cell Biosci *10*, 138. 10.1186/s13578-020-00493-1.
20. Wu, F., Fan, J., He, Y., Xiong, A., Yu, J., Li, Y., Zhang, Y., Zhao, W., Zhou, F., Li, W., et al. (2021). Single-cell profiling of tumor heterogeneity and the microenvironment in advanced non-small cell lung cancer. Nature Communications *12*, 2540. 10.1038/s41467-021-22801-0.
21. Yeh, H.-W., Hsu, E.-C., Lee, S.-S., Lang, Y.-D., Lin, Y.-C., Chang, C.-Y., Lee, S.-Y., Gu, D.-L., Shih, J.-H., Ho, C.-M., et al. (2018). PSPC1 mediates TGF-β1 autocrine signalling and Smad2/3 target switching to promote EMT, stemness and metastasis. Nature Cell Biology *20*, 479-491. 10.1038/s41556-018-0062-y.
22. Nieto, M.A., Huang, Ruby Y.-J., Jackson, Rebecca A., and Thiery, Jean P. (2016). EMT: 2016. Cell *166*, 21-45. 10.1016/j.cell.2016.06.028.
23. Takeuchi, Y., Tanegashima, T., Sato, E., Irie, T., Sai, A., Itahashi, K., Kumagai, S., Tada, Y., Togashi, Y., Koyama, S., et al. (2021). Highly immunogenic cancer cells require activation of the WNT pathway for immunological escape. Science Immunology *6*, eabc6424. doi:10.1126/sciimmunol.abc6424.
24. Grivennikov, S.I., Greten, F.R., and Karin, M. (2010). Immunity, Inflammation, and Cancer. Cell *140*, 883-899. 10.1016/j.cell.2010.01.025.

25. Simon, A.M., and Goodenough, D.A. (1998). Diverse functions of vertebrate gap junctions. Trends in Cell Biology *8*, 477-483. 10.1016/S0962-8924(98)01372-5.
26. Goodenough, D.A., and Paul, D.L. (2009). Gap Junctions. Cold Spring Harbor Perspectives in Biology *1*. 10.1101/cshperspect.a002576.
27. Zhang, C., and Schekman, R. (2023). Syncytin-mediated open-ended membrane tubular connections facilitate the intercellular transfer of cargos including Cas9 protein. eLife *12*, e84391. 10.7554/eLife.84391.
28. Platt, Randall J., Chen, S., Zhou, Y., Yim, Michael J., Swiech, L., Kempton, Hannah R., Dahlman, James E., Parnas, O., Eisenhaure, Thomas M., Jovanovic, M., et al. (2014). CRISPR-Cas9 Knockin Mice for Genome Editing and Cancer Modeling. Cell *159*, 440-455. 10.1016/j.cell.2014.09.014.
29. Jackson, E.L., Willis, N., Mercer, K., Bronson, R.T., Crowley, D., Montoya, R., Jacks, T., and Tuveson, D.A. (2001). Analysis of lung tumor initiation and progression using conditional expression of oncogenic K-ras. Genes & Development *15*, 3243-3248. 10.1101/gad.943001.
30. Lee, S.M., Schulz, C., Prabhash, K., Kowalski, D., Szczesna, A., Han, B., Rittmeyer, A., Talbot, T., Vicente, D., Califano, R., et al. (2023). First-line atezolizumab monotherapy versus single-agent chemotherapy in patients with non-small-cell lung cancer ineligible for treatment with a platinum-containing regimen (IPSOS): a phase 3, global, multicentre, open-label, randomised controlled study. The Lancet *402*, 451-463. https://doi.org/10.1016/S0140-6736(23)00774-2.
31. Waldman, A.D., Fritz, J.M., and Lenardo, M.J. (2020). A guide to cancer immunotherapy: from T cell basic science to clinical practice. Nature Reviews Immunology *20*, 651-668. 10.1038/s41577-020-0306-5.
32. Cadenas-De Miguel, S., Lucianer, G., and Elia, I. (2023). The metabolic cross-talk between cancer and T cells. Trends in Biochemical Sciences *48*, 597-609. 10.1016/j.tibs.2023.03.004.
33. Reinfeld, B.I., Madden, M.Z., Wolf, M.M., Chytil, A., Bader, J.E., Patterson, A.R., Sugiura, A., Cohen, A.S., Ali, A., Do, B.T., et al. (2021). Cell-programmed nutrient partitioning in the tumour microenvironment. Nature *593*, 282-288. 10.1038/s41586-021-03442-1.
34. Schmitt, C.A., Wang, B., and Demaria, M. (2022). Senescence and cancer — role and therapeutic opportunities. Nature Reviews Clinical Oncology *19*, 619-636. 10.1038/s41571-022-00668-4.
35. Kim, G., Shin, H.M., and Kim, H.-R. (2023). Pyrimidine nucleotide starvation induces a decrease in the number of effector T cells but not memory T cells. Cellular & Molecular Immunology *20*, 859-860. 10.1038/s41423-023-01014-z.
36. Lewis, J.R. (1974). Carbenoxolone sodium in the treatment of peptic ulcer. A review. Jama *229*, 460-462.
37. Lyssiotis, C.A., and Kimmelman, A.C. (2017). Metabolic Interactions in the Tumor Microenvironment. Trends Cell Biol *27*, 863-875. 10.1016/j.tcb.2017.06.003.
38. Hensley, Christopher T., Faubert, B., Yuan, Q., Lev-Cohain, N., Jin, E., Kim, J., Jiang, L., Ko, B., Skelton, R., Loudat, L., et al. (2016). Metabolic Heterogeneity in Human Lung Tumors. Cell *164*, 681-694. 10.1016/j.cell.2015.12.034.
39. Ackerman, D., and Simon, M.C. (2014). Hypoxia, lipids, and cancer: surviving the harsh tumor microenvironment. Trends in Cell Biology *24*, 472-478. https://doi.org/10.1016/j.tcb.2014.06.001.

40. Kumari, S., Advani, D., Sharma, S., Ambasta, R.K., and Kumar, P. (2021). Combinatorial therapy in tumor microenvironment: Where do we stand? Biochimica et Biophysica Acta (BBA) - Reviews on Cancer *1876*, 188585. https://doi.org/10.1016/j.bbcan.2021.188585.
41. Sciacovelli, M., Gonçalves, E., Johnson, T.I., Zecchini, V.R., da Costa, A.S.H., Gaude, E., Drubbel, A.V., Theobald, S.J., Abbo, S.R., Tran, M.G.B., et al. (2016). Fumarate is an epigenetic modifier that elicits epithelial-to-mesenchymal transition. Nature *537*, 544-547. 10.1038/nature19353.
42. Krieg, S., Fernandes, S.I., Kolliopoulos, C., Liu, M., and Fendt, S.-M. (2024). Metabolic Signaling in Cancer Metastasis. Cancer Discovery *14*, 934-952. 10.1158/2159-8290.Cd-24-0174.
43. Shaul, Yoav D., Freinkman, E., Comb, William C., Cantor, Jason R., Tam, Wai L., Thiru, P., Kim, D., Kanarek, N., Pacold, Michael E., Chen, Walter W., et al. (2014). Dihydropyrimidine Accumulation Is Required for the Epithelial-Mesenchymal Transition. Cell *158*, 1094-1109. https://doi.org/10.1016/j.cell.2014.07.032.
44. Siddiqui, A., Gollavilli, P.N., Schwab, A., Vazakidou, M.E., Ersan, P.G., Ramakrishnan, M., Pluim, D., Coggins, S.A., Saatci, O., Annaratone, L., et al. (2019). Thymidylate synthase maintains the de-differentiated state of triple negative breast cancers. Cell Death & Differentiation *26*, 2223-2236. 10.1038/s41418-019-0289-6.
45. Li, Q., Zhang, L., Yang, Q., Li, M., Pan, X., Xu, J., Zhong, C., Yao, F., Zhang, R., Zhou, S., et al. (2023). Thymidine kinase 1 drives hepatocellular carcinoma in enzyme-dependent and -independent manners. Cell Metabolism *35*, 912-927.e917. https://doi.org/10.1016/j.cmet.2023.03.017.
46. Siddiqui, M.A., Gollavilli, P.N., Ramesh, V., Parma, B., Schwab, A., Vazakidou, M.E., Natesan, R., Saatci, O., Rapa, I., Bironzo, P., et al. (2021). Thymidylate synthase drives the phenotypes of epithelial-to-mesenchymal transition in non-small cell lung cancer. British Journal of Cancer *124*, 281-289. 10.1038/s41416-020-01095-x.
47. Siddiqui, A., Vazakidou, M.E., Schwab, A., Napoli, F., Fernandez-Molina, C., Rapa, I., Stemmler, M.P., Volante, M., Brabletz, T., and Ceppi, P. (2017). Thymidylate synthase is functionally associated with ZEB1 and contributes to the epithelial-to-mesenchymal transition of cancer cells. J Pathol *242*, 221-233. 10.1002/path.4897.
48. Sahu, U., Villa, E., Reczek, C.R., Zhao, Z., O'Hara, B.P., Torno, M.D., Mishra, R., Shannon, W.D., Asara, J.M., Gao, P., et al. (2024). Pyrimidines maintain mitochondrial pyruvate oxidation to support de novo lipogenesis. Science *383*, 1484-1492. doi:10.1126/science.adh2771.
49. Skinner, O.S., Blanco-Fernández, J., Goodman, R.P., Kawakami, A., Shen, H., Kemény, L.V., Joesch-Cohen, L., Rees, M.G., Roth, J.A., Fisher, D.E., et al. (2023). Salvage of ribose from uridine or RNA supports glycolysis in nutrient-limited conditions. Nature Metabolism *5*, 765-776. 10.1038/s42255-023-00774-2.
50. Tabata, S., Yamamoto, M., Goto, H., Hirayama, A., Ohishi, M., Kuramoto, T., Mitsuhashi, A., Ikeda, R., Haraguchi, M., Kawahara, K., et al. (2017). Thymidine Catabolism as a Metabolic Strategy for Cancer Survival. Cell Reports *19*, 1313-1321. https://doi.org/10.1016/j.celrep.2017.04.061.
51. Nwosu, Z.C., Ward, M.H., Sajjakulnukit, P., Poudel, P., Ragulan, C., Kasperek, S., Radyk, M., Sutton, D., Menjivar, R.E., Andren, A., et al. (2023). Uridine-derived ribose fuels glucose-restricted pancreatic cancer. Nature *618*, 151-158. 10.1038/s41586-023-06073-w.

940